Electronic Supplementary Material (ESI) for ChemComm.

Thienyl-BOPHY Dyes as Promising Templates for Bulk Heterojunction Solar Cells

A. Mirloup,[a] Q. Huaulmé,[a] N. Leclerc,[b] P. Lévêque,[c] T. Heiser,[c] P. Retailleau,[d] R. Ziessel,[a]

Supporting Information

Table of Contents

1) General Methods

Optical Measurements.

Absorption spectra were recorded on a Schimadzu UV-3000 absorption spectrometer. The steady-state fluorescence emission and excitation spectra were obtained by using a

HORIBA JOBIN YVON FLUOROMAX 4. All fluorescence spectra were corrected. The fluorescence quantum yield (ϕ_{exp}) was calculated from eq. 1.

$$\Phi_{cmp} = \Phi_{ref} \frac{I}{I_{ref}} \frac{OD_{ref}}{OD} \frac{\eta^2}{\eta_{ref}{}^2} \text{ (equation 1)}$$

Here, I denote the integral of the corrected emission spectrum, OD is the optical density at the excitation wavelength and η is the refractive index of the medium. The reference systems used were rhodamine 6G (Φref = 0.78) in air equilibrated water and Tetramethoxydiisoindomethene-difluoroborate (Φref = 0.51).[2] Luminescence lifetimes were measured on an Edimburgh Instruments spectrofluorimeter equipped with a R928 photomultiplier and a PicoQuant PDL 800-D pulsed diode connected to a GwInstect GFG-8015G delay generator. No filter was used for the excitation. Emission wavelengths were selected by a monochromator. Lifetimes were deconvoluted with FS-900 software using a light-scattering solution (LUDOX) for instrument response.

Electrochemical Measurements.

Electrochemical studies employed cyclic voltammetry with a conventional 3-electrode system using a BAS CV-50W voltammetric analyser equipped with a Pt microdisk (2 mm^2) working electrode and a silver wire counter-electrode. Ferrocene was used as an internal standard and was calibrated against a saturated calomel reference electrode (SCE) separated from the electrolysis cell by a glass frit presoaked with electrolyte solution. Solutions contained the electro-active substrate in deoxygenated and anhydrous dichloromethane containing tetra-n-butylammonium hexafluorophosphate (0.1 M) as supporting electrolyte. The quoted half-wave potentials were reproducible within ≈ 15 mV.

2) Synthetic Experimental Part

Corresponding mono-thienyl and bis-thieneyl aldehydes were prepared using established protocols.[S1]

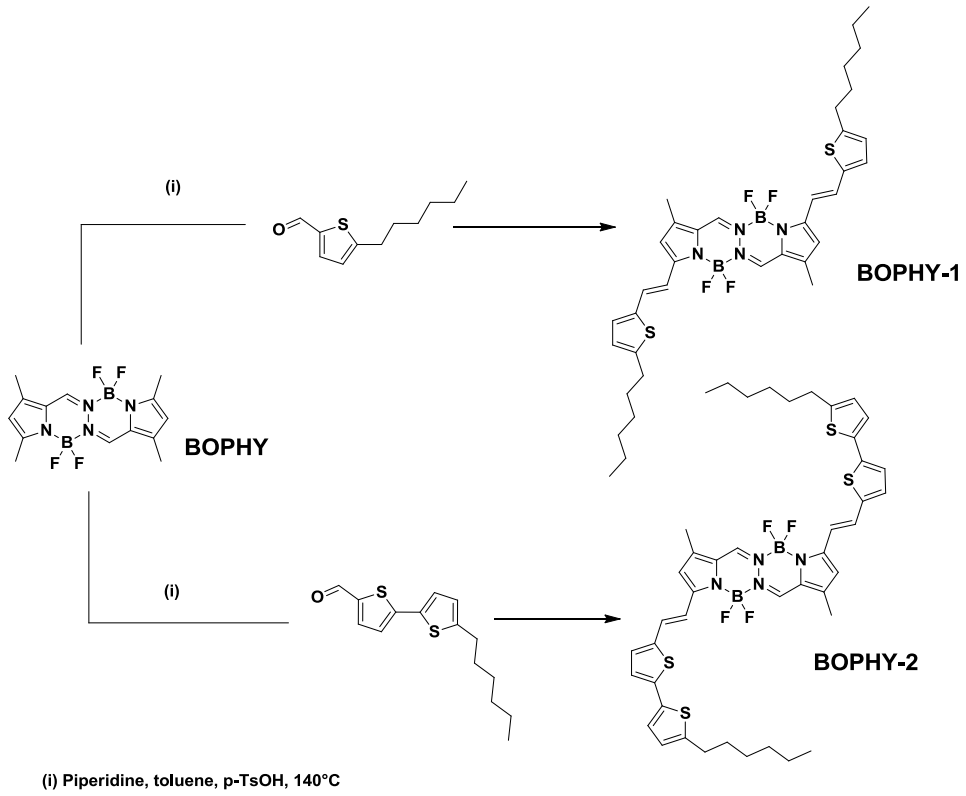

Scheme S1.

General procedure for the Knoevenagel condensations: A solution of BOPHY, aldehyde (3.0 equiv.) and a crystal a *p*-TsOH in toluene (5 ml) and piperidine (1 ml) was heated at 140 °C and the solvents were evaporated until dryness. The mixture was diluted with dichloromethane and washed with water. The aqueous phase was extracted with dichloromethane. The combined organic phase was dried over $MgSO_4$ or absorbent cotton and the solvents were evaporated under reduced pressure. The crude product was purified by column chromatography and recrystallized by slow diffusion of pentane in THF.

BOPHY-1.

Reaction was performed on 136 mg of BOPHY. Column chromatography on Silica gel (Petroleum ether/dichloromethane (v/v): 60/40) followed by recrystallization by diffusion of pentane in a concentrated THF solution afforded 76 mg of the pure expected product (29%, dark violet solid). ^{1}H NMR (400 MHz, $CDCl_3$): δ = 7.92 (s, 2H), 7.32 (d, ^{3}J = 15.7Hz, 2H), 7.08 (d, ^{3}J = 15.7 Hz, 2H), 7.00 (d, ^{3}J = 3.6 Hz, 2H), 6.71 (d, ^{3}J = 3.6 Hz, 2H), 6.67 (s, 2H), 2.81 (t, ^{3}J = 7.6 Hz, 4H), 2.35 (s, 6H), 1.69 (q, ^{3}J = 7.6 Hz, 4H), 1.29-1.41 (m, 12H), 0.90 (t, 6.7 Hz, 6H). ^{13}C NMR (100 MHz, $CDCl_3$): 149.8, 149.1, 140.4, 139.7, 132.9, 129.9, 129.1, 125.4, 125.0, 115.9, 114.9, 31.7, 31.6, 30.7, 28.9, 22.7, 14.2, 11.3. ^{11}B NMR (128 MHz, $CDCl_3$): 0.98 .^{19}F NMR (375 MHz, $CDCl_3$): -140.9 (d, $J_{(B\text{-}F)}$=42.1Hz). Anal. Calcd for (Mr = 694.51): C, 62.26; H, 6.39; N, 8.07; Found: C, 62.07; H, 6.29; N, 7.84. ESI-MS, m/z (%): 695.2 ([M+1], 100), 675.2 (30), 656.1 (15).

BOPHY-2.

Reaction was performed on 106 mg of BOPHY. Column chromatography on Silica gel (Petroleum ether/toluene/dichloromethane (v/v/v): 50/40/10) followed by recrystallization by diffusion of pentane in a concentrated THF solution afforded 53 mg of the pure expected product (21%, dark blue solid). ^{1}H NMR (400 MHz, $CDCl_3$): δ = 7.94 (s, 2H), 7.33 (d, ^{3}J = 16.3 Hz, 2H), 7.12 (d, ^{3}J = 16.3 Hz, 2H), 7.06 (d, ^{3}J = 3.5 Hz, 2H), 7.04 (d, ^{3}J = 3.4 Hz, 2H), 7.02 (d, ^{3}J = 3.5 Hz, 2H), 6.70 (d, ^{3}J = 3.4 Hz, 2H), 6.95 (s, 2H), 2.80 (t, ^{3}J = 7.6 Hz, 4H), 2.36 (s, 6H), 1.69 (q, ^{3}J = 7.3 Hz, 4H), 1.30-1.41 (m, 12H), 0.90 (t, ^{3}J = 6.9 Hz, 6H). ^{13}C NMR (100 MHz, $CDCl_3$): 149.5, 146.7, 140.5, 140.1, 140.0, 134.6, 132.9, 130.0, 129.3, 125.3, 125.2, 124.3, 123.7, 116.6, 115.1, 31.7, 31.6, 30.4, 28.9, 22.7, 14.2, 11.3. ^{11}B NMR (128 MHz, $CDCl_3$): 0.90. ^{19}F NMR (375 MHz, $CDCl_3$): -140.7 (d, $J_{(B\text{-}F)}$=42.8 Hz). Anal. Calcd for (Mr = 858.75): C, 61.54; H, 5.63; N, 6.52; Found: C, 61.31; H, 5.42; N, 6.37. ESI-MS, m/z (%): 859.1 ([M+1], 100), 839.1 (30), 820.1 (20).

3) NMR Traces

Figure S1: ^{1}H NMR spectrum of BOPHY-1 (400 MHz, $CDCl_3$, 273K).

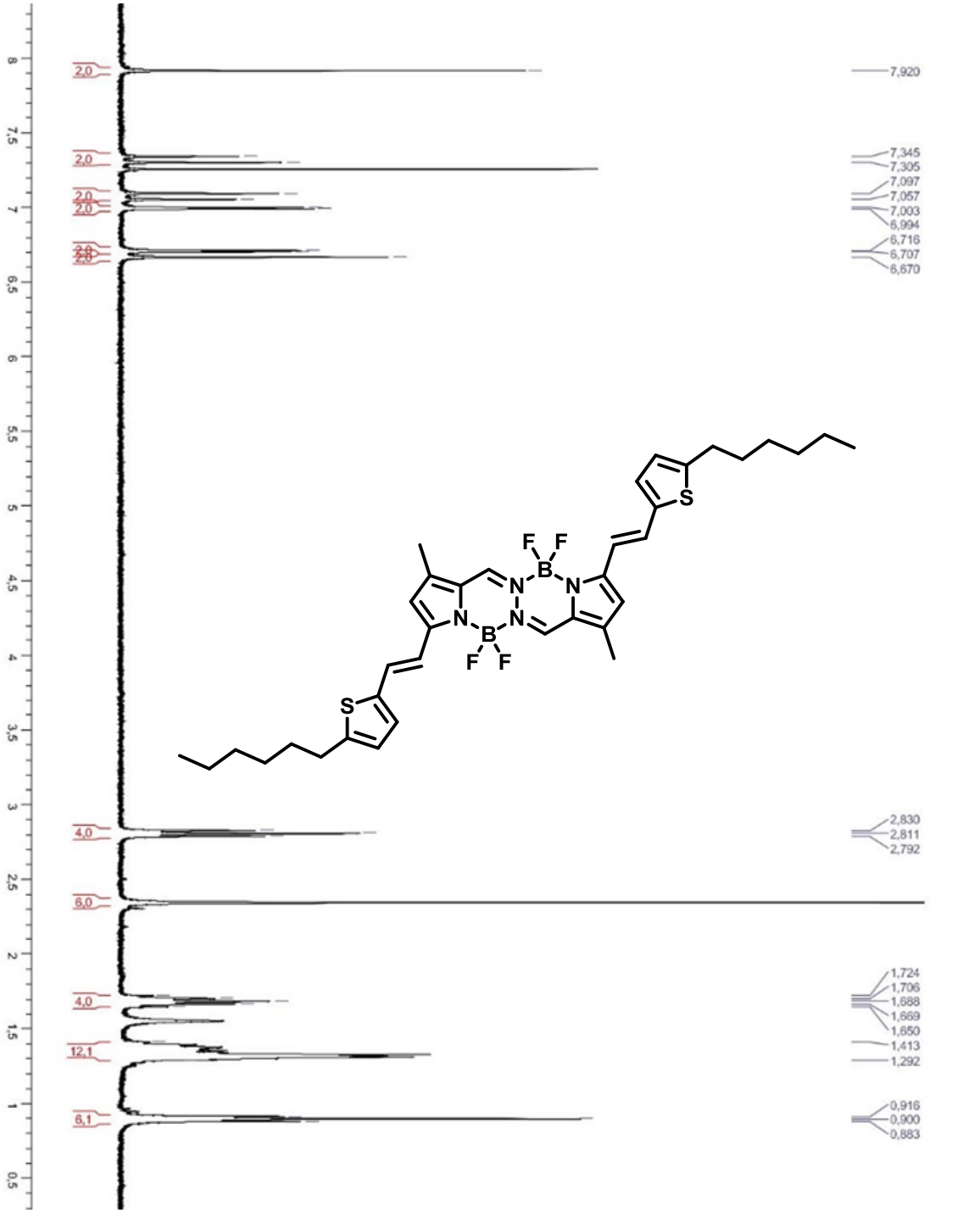

Figure S2: ^{13}C NMR spectrum of BOPHY-1 (100 MHz, $CDCl_3$, 273K).

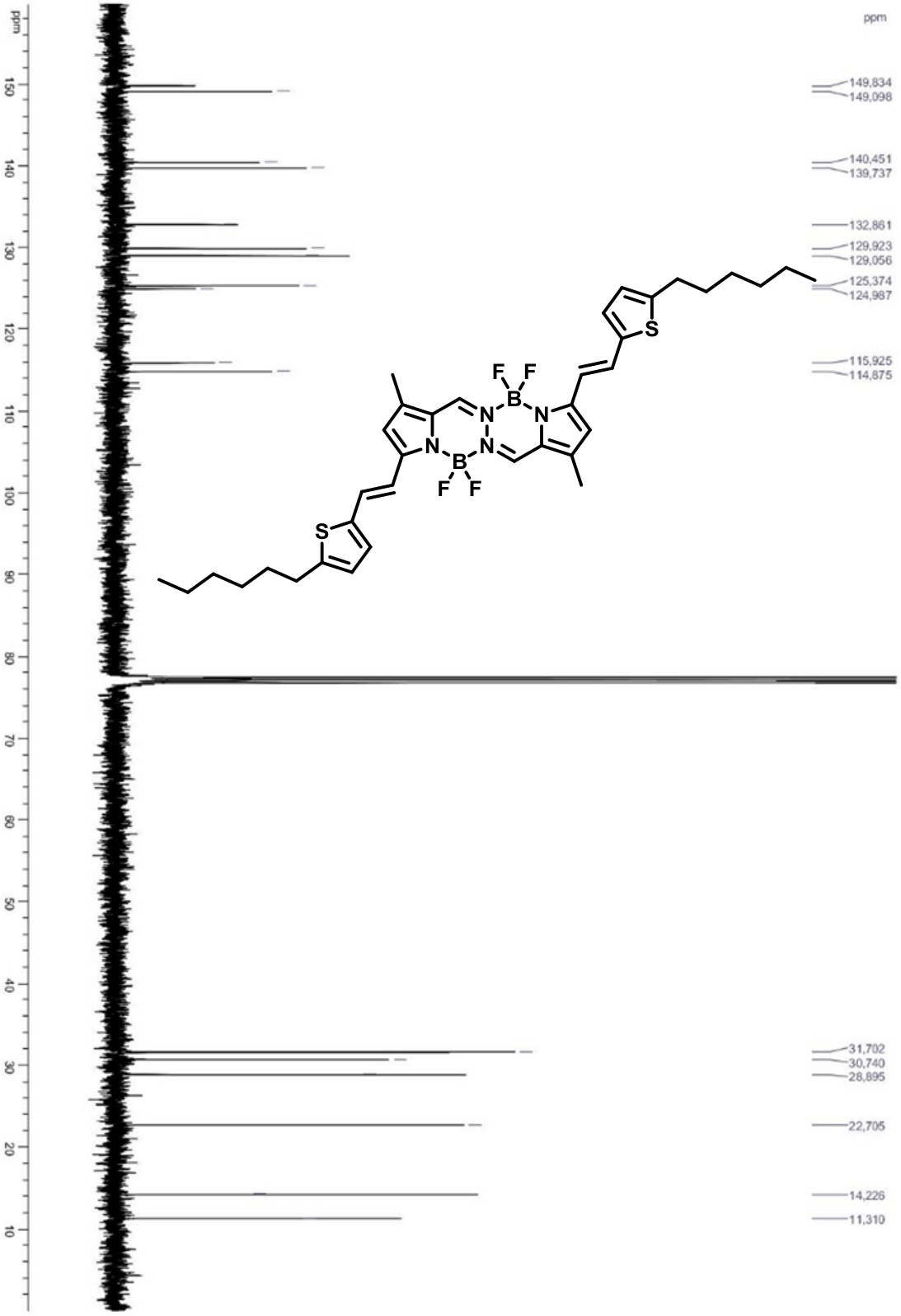

Figure S3: ^{11}B NMR spectrum of BOPHY-1 (128 MHz, $CDCl_3$, 273K).

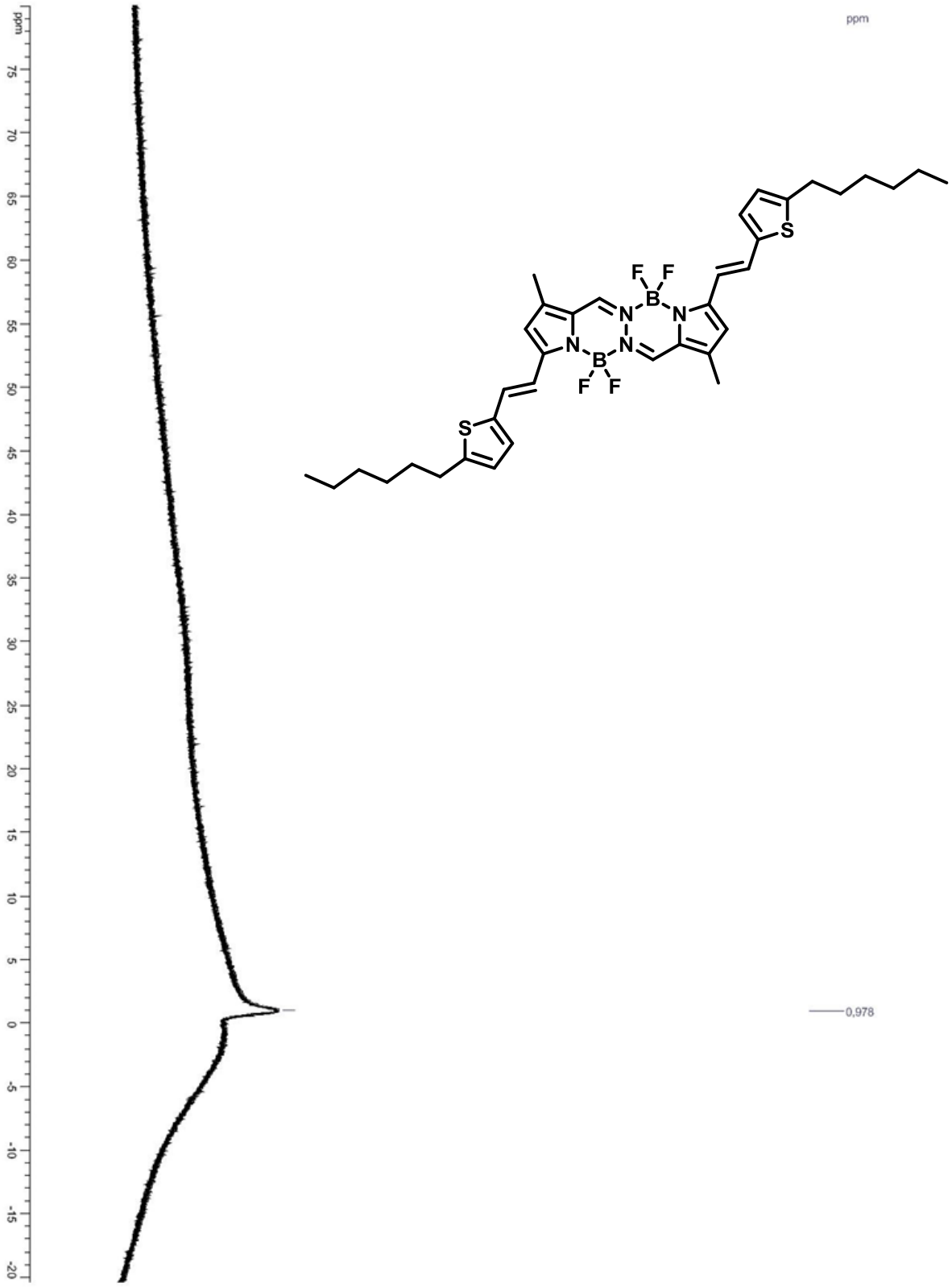

Figure S4: ^{19}F NMR spectrum of BOPHY-1 (375 MHz, $CDCl_3$, 273K).

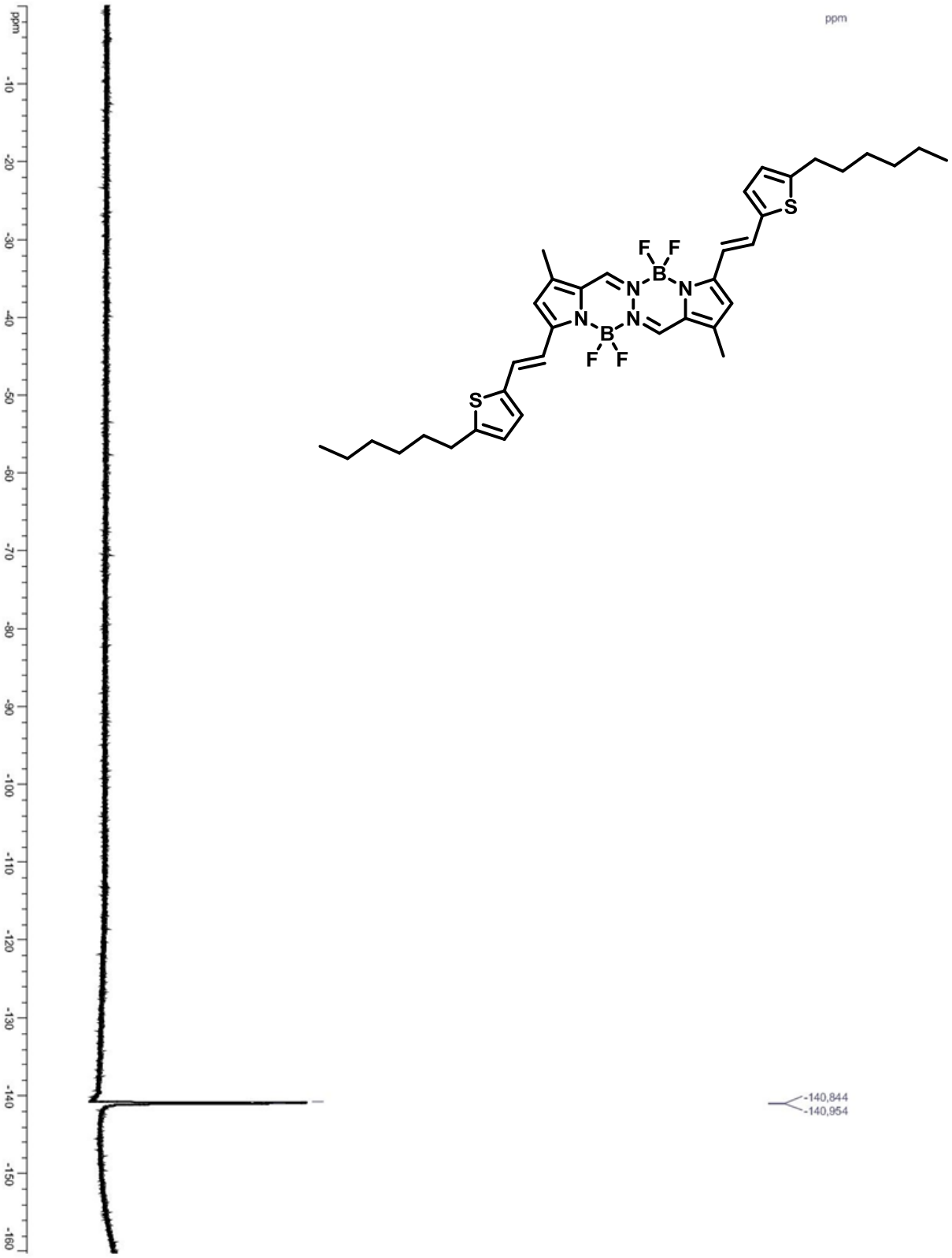

Figure S5: ^{1}H NMR spectrum of BOPHY-2 (400 MHz, $CDCl_3$, 273K).

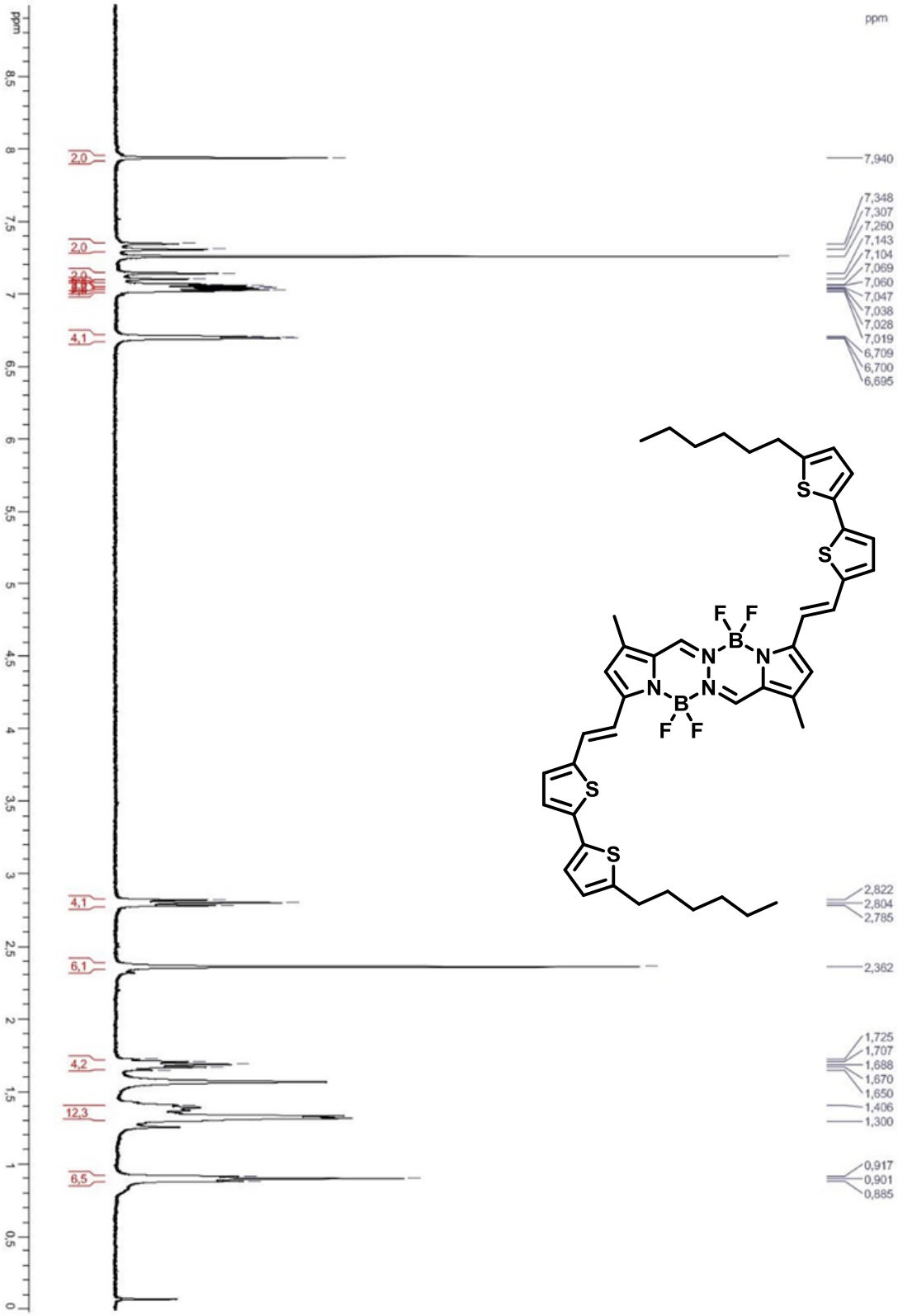

Figure S6: ^{13}C NMR spectrum of BOPHY-2 (100 MHz, $CDCl_3$, 273K).

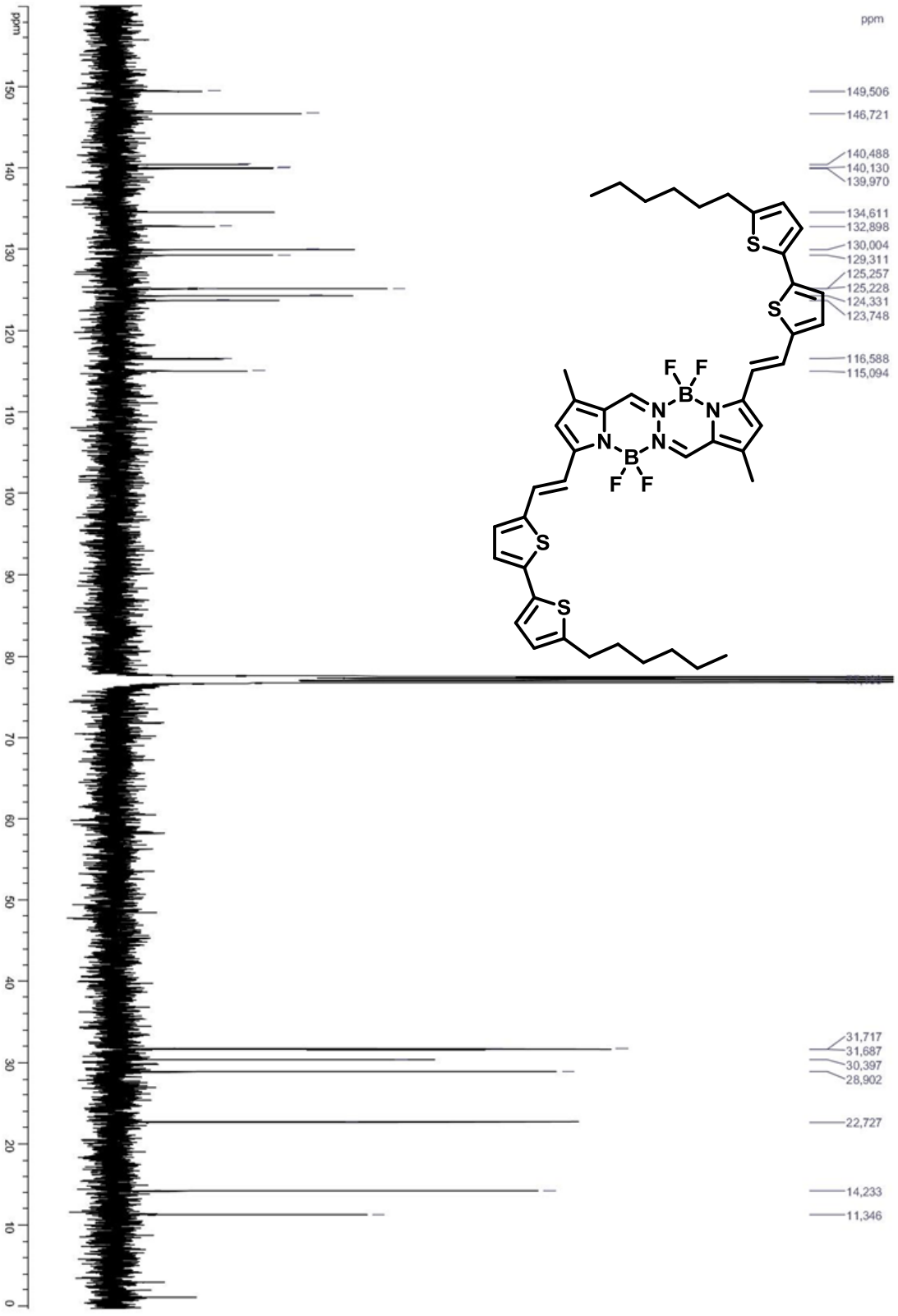

Figure S7: ^{11}B NMR spectrum of BOPHY-1 (128 MHz, $CDCl_3$, 273K).

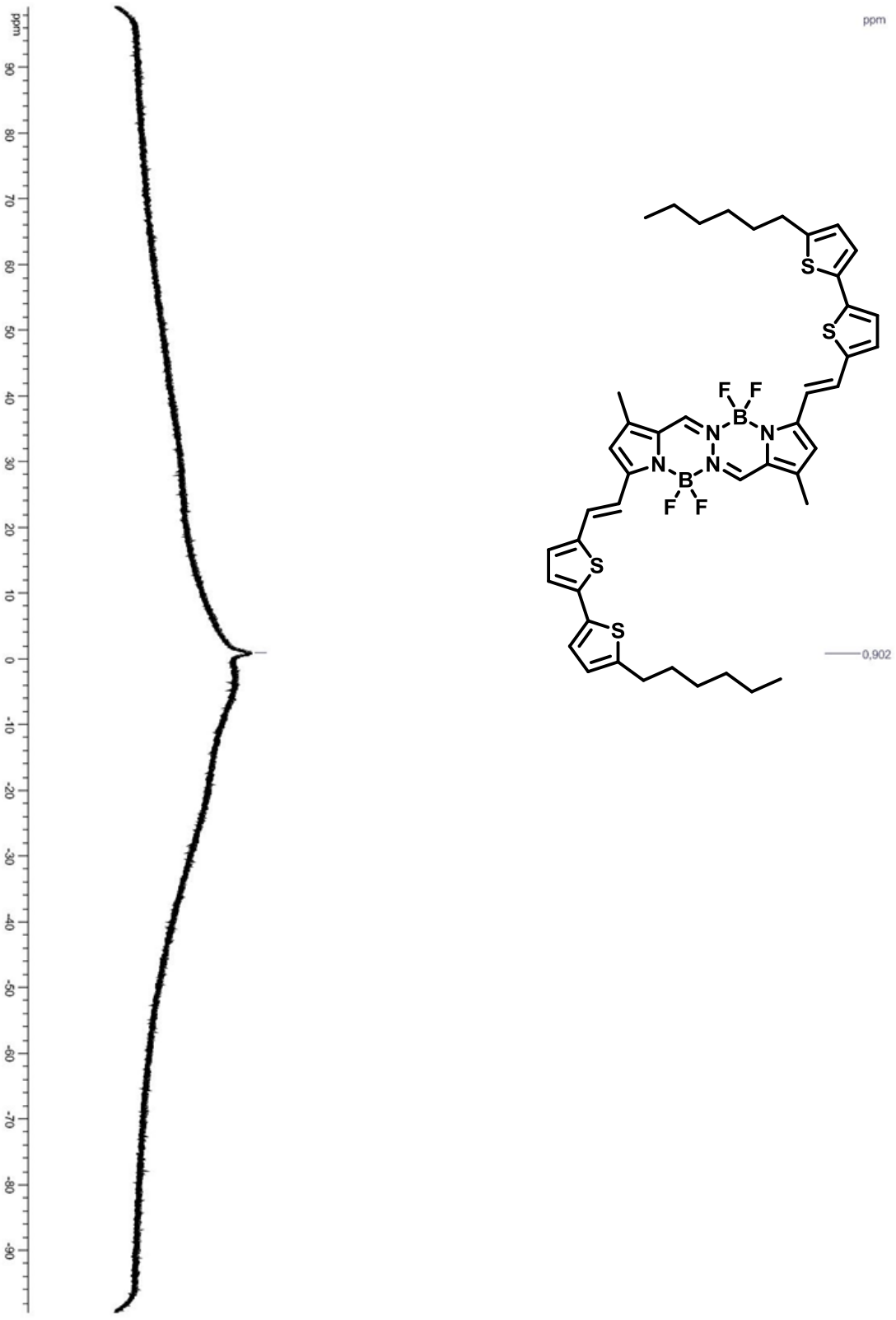

Figure S8: ^{19}F NMR spectrum of BOPHY-1 (375 MHz, $CDCl_3$, 273K).

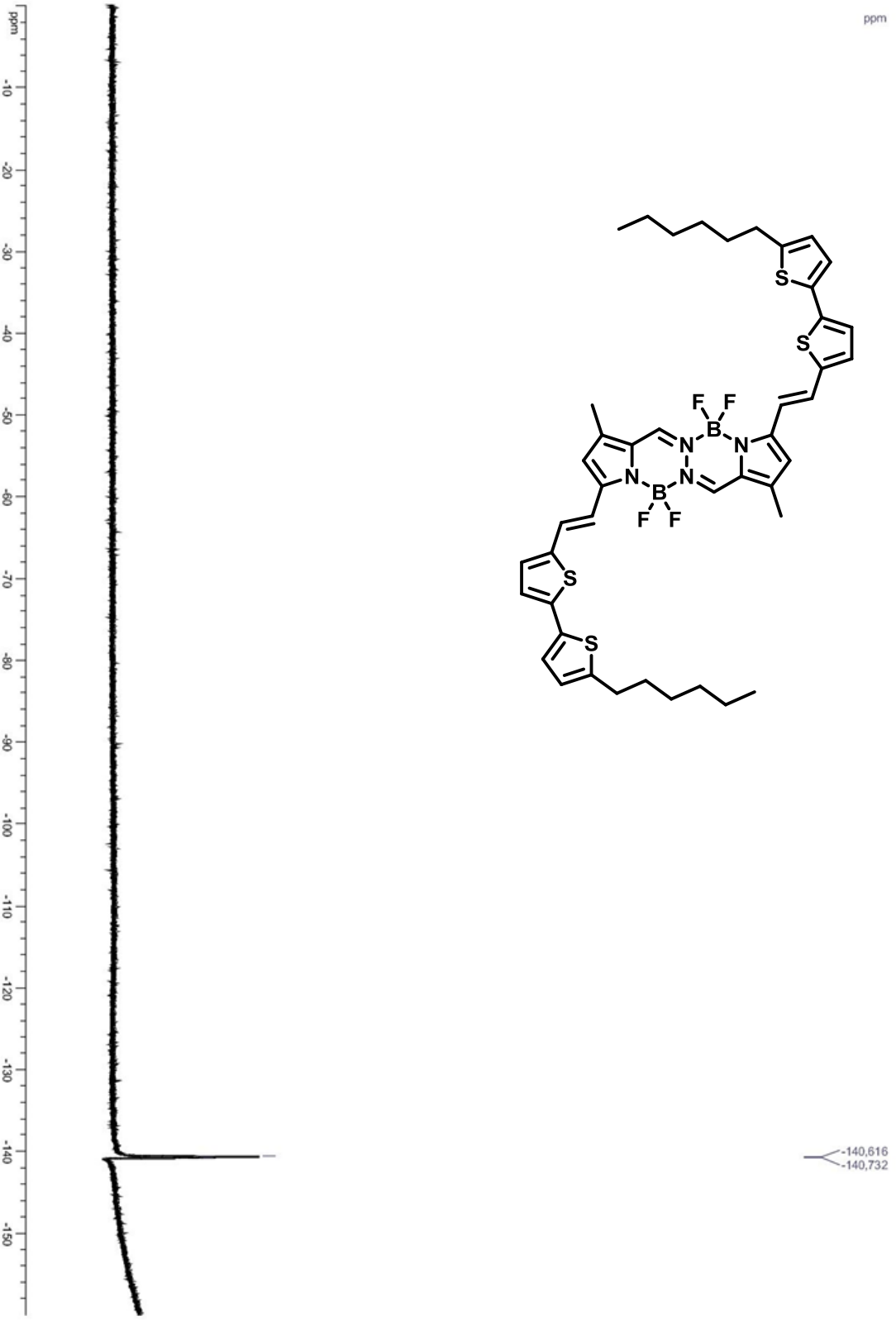

4) Crystallographic data

Table S1. Crystal data and Structure refinement for **BOPHY-2**.

Identification code		**BOPHY-2**
CRYSTAL DATA		
Empirical formula		$C_{44}\ H_{48}\ B_2\ F_4\ N_4\ S_4$
Formula weight		858.72
Crystal system		Triclinic
Space group		P -1
Unit cell dimensions	*a* (Å)	8.3989(2)
	b (Å)	14.2716(4)
	c (Å)	18.5507(13)
	α (°)	94.761(7)
	β (°)	96.451(7)
	γ (°)	101.646(7)
Volume (Å^3)		2151.23(18)
Z, Z'		2, 1
*Calcd density (*Mg/m^3)		1.326
Wavelength (Å)		1.54187
Abs. coefficient μ (mm^{-1})		2.428
F(000)		900
DATA COLLECTION		
Crystal habit and size (mm)		Dark violet plate 0.42 x 0.22 x 0.08
Diffractometer		Rapid II mm007HF – CMF optics
Temperature (K)		213(2)
θ range for data collection (°)		2.41 to 58.93
Limiting indices		-8 ≤ h ≤ 9, -15≤ k ≤ 15, -19 ≤ l ≤ 20
Reflect° collected / unique		17489 / 6004
R(int)		0.0714
Completeness to θ $_{max}$ (%)		96.9
Absorption correction		Semi-empirical from equivalents
Max. and min. transmission		0.82 and 0.61
SOLUTION and REFINEMENT		
Solution method		Direct Methods
Refinement method		Full-matrix least-squares on F^2
Data / restraints / parameters		6007 / 0 / 527
Goodness-of-fit on F^2		0.944
Final R indices [I>2σ(I)]	R1	0.059
	wR2	0.1339
R indices (all data)	R1	0.1764
	wR2	0.1979
Largest Δ peak and hole (e.Å^3)		0.967 and -1.030
CCDC deposit number		1045172

Computing Software for :

Data Collection, Cell Refinement and Data Reduction: CrystalClear-SM Expert 2.0 r4/Fs_Process, Fs-Abscor (Rigaku, 2009).[S2] Structure_Solution: SHELXS97 (Sheldrick, 2008).[S3] Structure Refinement: SHELXL2014 (Sheldrick, 2015)[S4]; SHEXLE (Hübschle et al, 2011).[S5] Molecular_Graphics : ORTEP-III (Burnett and Johnson, 1996)[S7]; PLATON (Spek, 2009).[S6]

Figure S9: View of crystal layer with different colours to emphasize the sparsed π-π interactions in the crystal (blue spots between A and B layers, red spots between B and C).

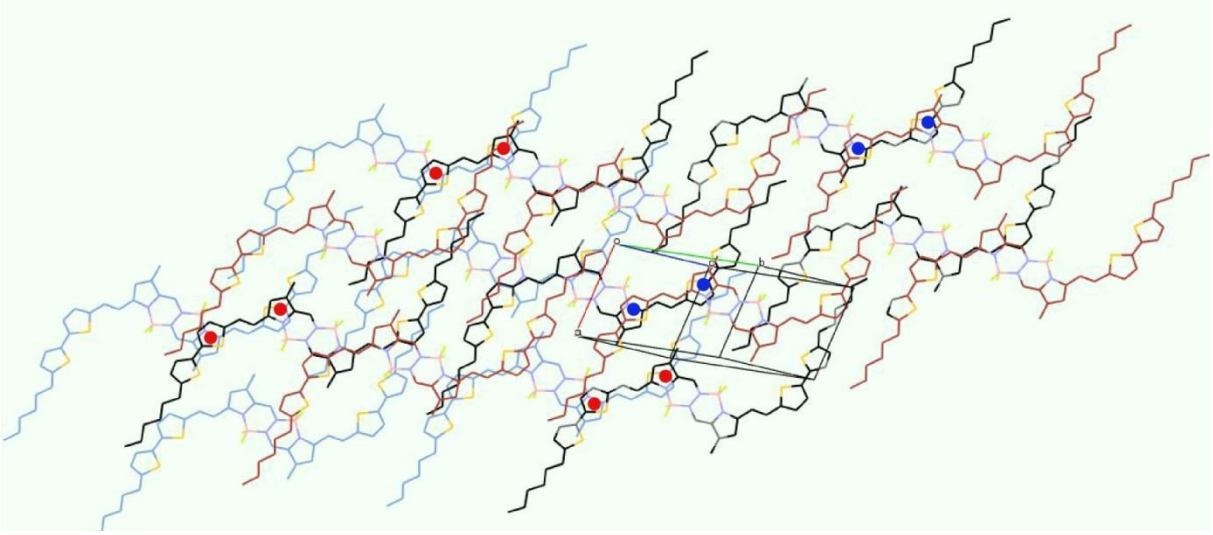

5) Spectroscopic data

Figure S10: Absorption (red trace), emission (green trace, λ_{exc} = 550 nm) and excitation (dashed black trace, λ_{emi} = 627 nm) spectra of **BOPHY-1**, in THF at room temperature (C = 8.16 x 10^{-6} M).

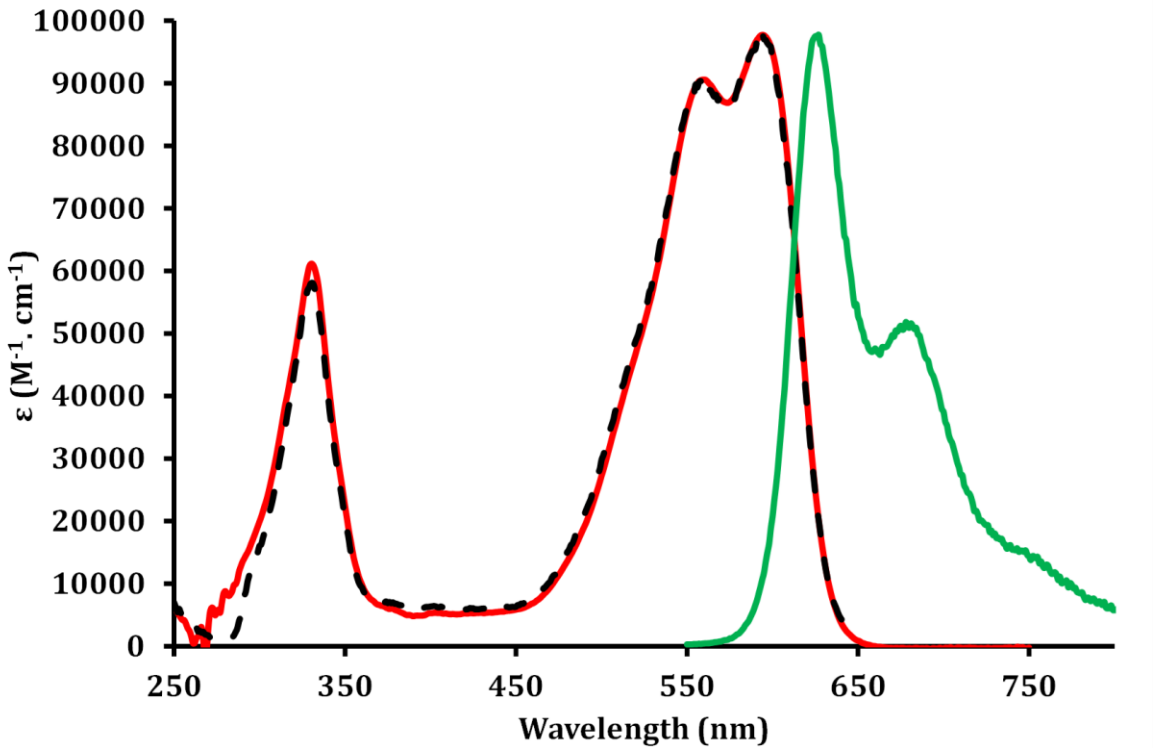

Figure S11: Absorption (red trace), emission (green trace, λ_{exc} = 550 nm) and excitation (dashed black trace, λ_{emi} = 674 nm) spectra of **BOPHY-2**, in THF at room temperature (C = 4.66 x 10^{-6} M).

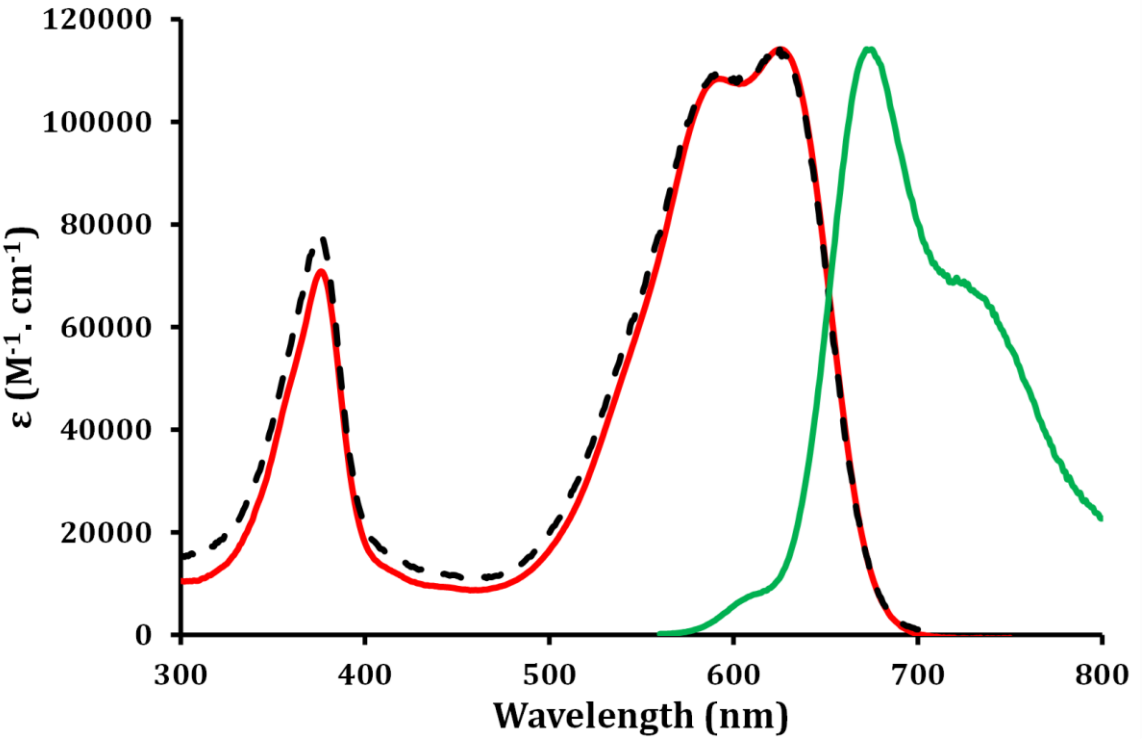

Table S2. Selected spectroscopic data for **BOPHY-1** and **BOPHY-2** dyes.

Compound	λ_{abs} sol (nm)	λ_{abs} film (nm)	ε ($M^{-1}.cm^{-1}$)	λ_{em} solution (nm)	Φ_F (λ_{ex}, nm) [a]	τ (ns)	k_r (10^7 s^{-1}) [b]	k_{nr} (10^7 s^{-1}) [c]	Δss (cm^{-1}) [d]	FWHM sol (cm^{-1}) [e]	FWHM film (cm^{-1}) [e]	Optical gap (eV) [f]
BOPHY-1	595	620	97,000	627	0.13 (@530)	1.38	9.42	63.0	860	2,900	7,000	1.69
BOPHY-2	626	651	113,000	674	0.10 (@550)	0.68	16.4	148	1,100	3,000	6,300	1.62

[a] ϕ_F was calculated from $\Phi_{exp} = \Phi_{ref} \frac{I}{I_{Ref}} \frac{OD_{Ref}}{OD} \frac{\eta^2}{{\eta_{Ref}}^2}$ with rhodamine 6G (Φref = 0.78)[S8] in air equilibrated water and Tetramethoxydiisoindomethene-difluoroborate (Φref = 0.51) as references. [b] k_r was calculated from $\Phi_F = \frac{k_r}{k_r+k_{nr}} = k_r\tau$. [c] k_{nr} was calculated from $k_{nr} = \frac{1-\Phi_F}{k_r}$. [d] Stokes shifts. [e] Full width at half maximum. [f] Measured from the absorption onset at the low energy side of the absorption spectrum in thin film.

6) Electrochemical data

Table S3. Selected electrochemical data for **BOPHY-1** and **BOPHY-2** dyes.[a)]

Compound	$E_{1/2}$ ox (mV)	$E_{1/2}$ red (mV)	E_{ox} onset (mV)	E_{red} onset (mV)	HOMO (eV)	LUMO (eV)	Electrochemical gap (eV)
BOPHY-1	922	-1,110	730	-1,055	-5.51	-3.73	1.78
BOPHY-2	814	-1,057	720	-994	-5.50	-3.79	1.78

a) Potentials determined by cyclic voltammetry in deoxygenated dichloromethane solution, containing 0.1 M $TBAPF_6$, [electrochemical window from +1.7 to -2.3 V], at a solute concentration of ca. 1.5 mM and at rt. Potentials were standardized versus ferrocene (Fc) as internal reference and converted to the SCE scale assuming that $E_{1/2}$ (Fc/Fc^+) = +0.38 V (ΔEp = 60 mV) *vs* SCE. Error in half-wave potentials is ±15 mV. For irreversible processes the peak potentials (E_{ap}) are quoted. All reversible redox steps result from one-electron processes.

7) DFT Calculations

Density functional theory at the B3LYP/6-311+G* level of theory in vacuum (using Spartan 10[S9]) was utilized to model the structural and electronic properties of relevant molecular structures. In particular, the HOMO, LUMO and LUMO+1 level positions and related electron distributions were calculated. To keep the computational time within a reasonable range, the alkyl chains were replaced by methyl groups. It is thereby assumed that the electronic coupling between alkyl chains and the π-electron system is negligible.

Figure S12: Calculated HOMO, LUMO and LUMO+1 distribution for the BOPHY-1 dye.

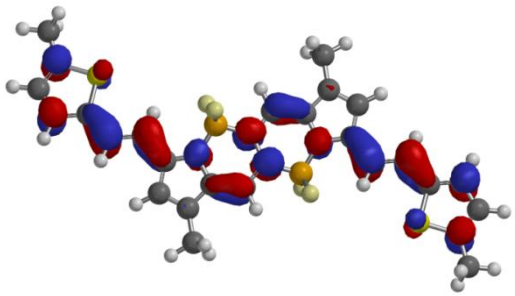

BOPHY-1: LUMO+1

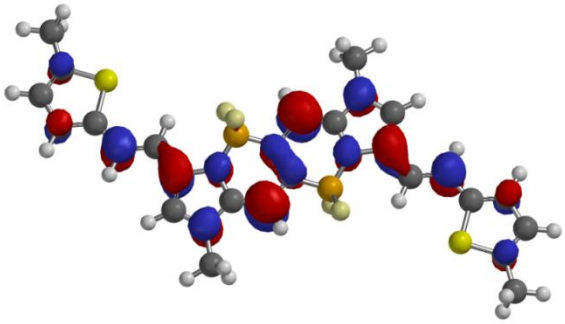

BOPHY-1: LUMO

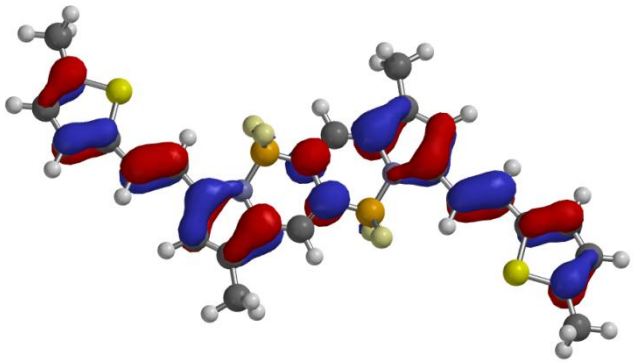

BOPHY-1: HOMO

Figure S13: Calculated HOMO, LUMO and LUMO+1 distribution for the BOPHY-2 dye.

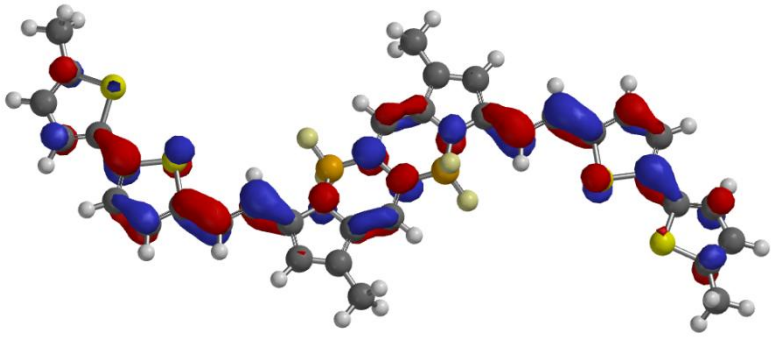

BOPHY-2: LUMO+1

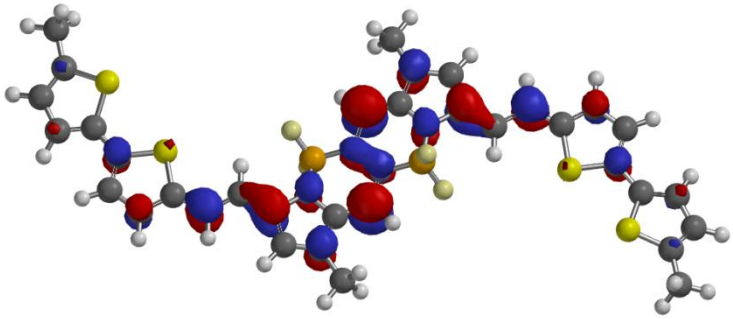

BOPHY-2: LUMO

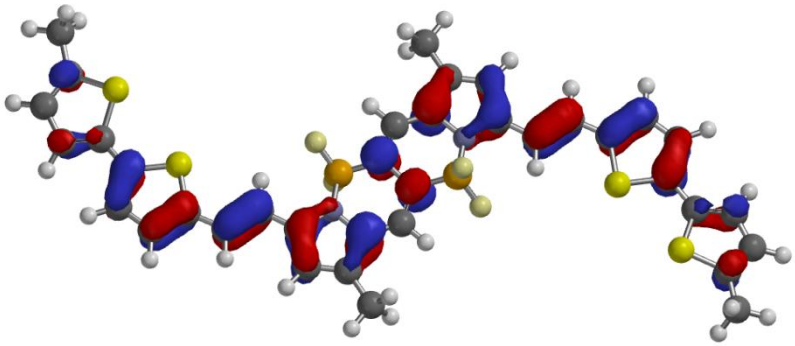

BOPHY-2: HOMO

8) DSC Measurements

DSC measurements were performed with a TA Instruments Q1000 instrument, operated at a scanning rate of 5 °C min-1 on heating and on cooling.

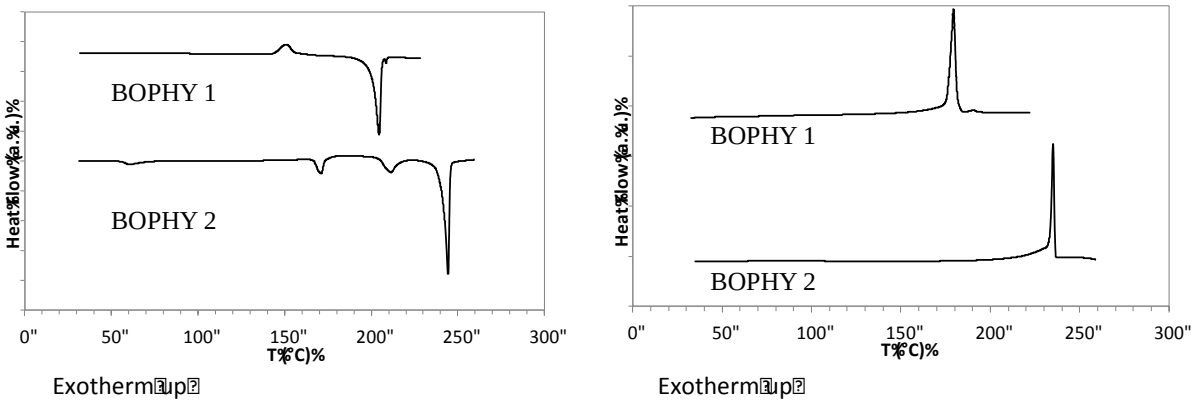

Figure S14: Second heating (left) and cooling (right) DSC traces at 5°C/Min. During the heating, the large peak corresponds to the transition to the isotropic liquid, occurring at 204°C and 244°C for BOPHY-1 and BOPHY-2, respectively. DSC traces of BOPHY-2 show several transitions between crystalline phases, which are not visible by POM.

9) Field effect transistors and Photovoltaic characterizations

Field effect transport measurements.

Bottom contact field-effect transistors (FETs) were elaborated on commercially available pre-patterned test structures whose source and drain contacts were composed of a 30 nm thick gold layer on top of a 10 nm thick Indium Tin Oxide (ITO) layer. A 230 nm thick silicon oxide was used as gate dielectric and n-doped ($3x10^{17}/cm^3$) silicon crystal as gate electrode. The channel length and channel width were 20 µm and 10 mm, respectively. The test structures were cleaned in acetone and isopropyl alcohol and subsequently for 30 minutes in an ultra-violet ozone system. Then, hexamethyldisilazane (HMDS) was spin-coated (500 rpm for 5 s and then 4000 rpm for 50 s) under nitrogen ambient followed by an annealing step at 130°C for 10 minutes. Finally, 5 mg/mL anhydrous chloroform of dyes solutions were spin coated (1250 rpm for 60 s and 2250 rpm for 60 s) to complete the FET devices. The samples were then left overnight under vacuum ($<10^{-6}$ mbar) to remove residual solvent traces. Both, the FET elaboration and characterizations were performed in nitrogen ambient. The transistor output and transfer characteristics were recorded using a Keithley 4200 semiconductor characterization system. The charge carrier mobility was extracted in the linear and saturation regime using the usual formalism on FET devices annealed at the same temperature as the optimized photovoltaic devices. Nevertheless, the measured hole mobility before or after a (5 minutes, 70°C) thermal annealing were in the same range within the experimental uncertainty (estimated as $1x10^{-5}$ $cm^2/V.s$ for each dye). On the other hand, after a thermal treatment at 90°C for 10 minutes, the measured hole-mobility drops by an order of magnitude for both dyes.

Table S4. OFETs hole mobilities for BOPHY-1 and BOPHY-2.

Dye	Annealing	μ_{lin} (cm²/V.s)	μ_{sat} (cm²/V.s)
BOPHY-1	/	$7x10^{-5}$	$9x10^{-4}$
BOPHY-2	5 min 70°C	$3x10^{-5}$	$5x10^{-5}$

Figure S15: Output characteristics for OFETs with a BOPHY-1 dye channel (left) or a BOPHY-2 channel (right).

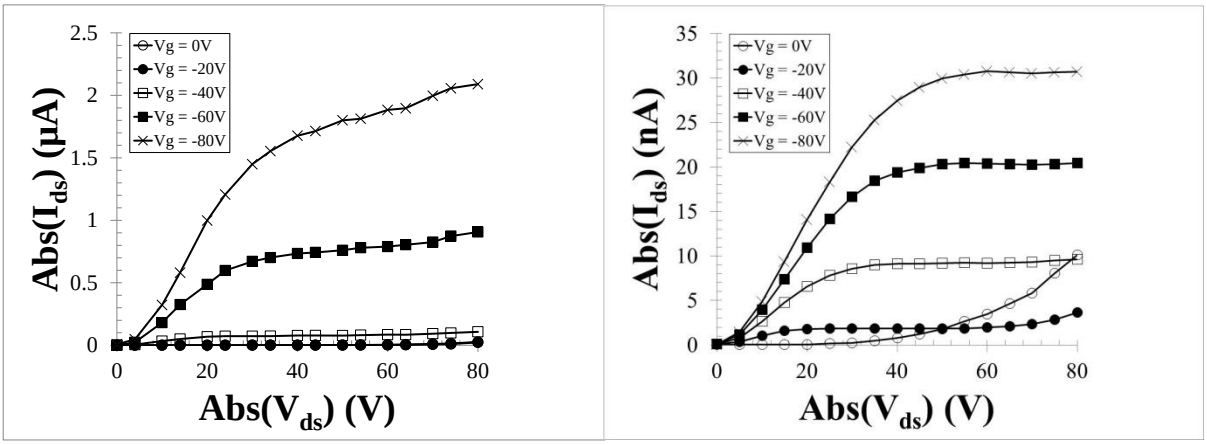

BOPHY-2 exhibits output characteristics typical for an ambipolar behavior. Both dyes shows a non negligible series resistance that may lead to an underestimation of the mobilities.

Photovoltaic devices preparation.

Bulk heterojunction devices were elaborated using the different synthesized molecules as electron-donor and $PC_{71}BM$ as electron-acceptor with and without diiodooctane (DIO) as additive. Standard solar cells were elaborated by using the following device structure: ITO/PEDOT-PSS(40 nm)/electron-donor molecule:$PC_{71}BM$/Ca(20 nm)Al(120 nm). Indium Tin Oxide coated glass with a surface resistance lower than 20 Ω/sq was used as transparent substrate. Substrates were cleaned sequentially by ultrasonic treatments in acetone, isopropyl alcohol, and deionized water. After an additional cleaning for 30 minutes under ultra-violet generated ozone, PEDOT-PSS or PEIE (M_W=70000 g/mol) were spin coated at 1500 rpm for 60s or 5000 rpm for 60s, respectively. Finally, PEDOT-PSS was thermally annealed for 30 minutes at 140°C under nitrogen atmosphere. The organic solvent dye:$PC_{71}BM$ solutions were stirred for at least 24 hours at 50°C before spin-coating. An extra stirring for 15 minutes at 100°C was added just before the active layer deposition. In the following are reported the best conditions leading to optimal devices for each molecule. Thus, the molecule BOPHY-1 has been deposited from a chloroform solution at the concentration of 15 mg/mL. The molecule BOPHY-2 has been deposited from a chloroform solution at the concentration

of 10 mg/mL. All molecules active layers have been spin-coated in the following conditions: a first 120 seconds step (speed: 2000 rpm, acceleration: 600 rpm/s) followed by a second 60 seconds step (speed: 2500 rpm, acceleration: 600 rpm/s). A post-deposition thermal annealing process (for 0 to 2 minutes at 70°C) was added before the cathode thermal evaporation. Each device contained four 12 mm^2 diodes, the surface of each diode being carefully defined by a shadow mask. The photovoltaic cells elaboration after substrate preparation was performed in nitrogen ambient.

Photovoltaic measurements.

Current versus Voltage (J-V) characteristics were measured using a source measurement unit Keithley 2400 under darkness and under AM1.5G (100 mW/cm^2) illumination. The standard illumination was provided by a Class A Lot Oriel solar simulator (550 W filtered Xe lamp) and the illumination power was calibrated using a reference silicon solar cell. Photovoltaic measurements were also performed with different light intensities using neutral filters with different absorption coefficient. External Quantum Efficiency (EQE) measurements were performed using a home-made setup including a 150 W Lot Oriel Xe solar simulator as a light source, a Jobin-Yvon microHR monochromator and several focusing lenses to obtain a 2 mm diameter monochromatic light beam on the solar cell under investigation. Calibrated silicon reference cells were used to monitor the incident and the reflected light power for each wavelength. All the characterizations were performed in nitrogen ambient.

Figure S16. Best (J-V) curves measured using BOPHY-1 (a) or BOPHY-2 (b) as electron-donor molecules. The curves were obtained in the dark (closed symbols) or under standard AM1.5G (100 mW/cm^2) (open symbols) without (circles) or with (squares) DIO as additive. The device parameters and main experimental conditions can be found in Table 1.

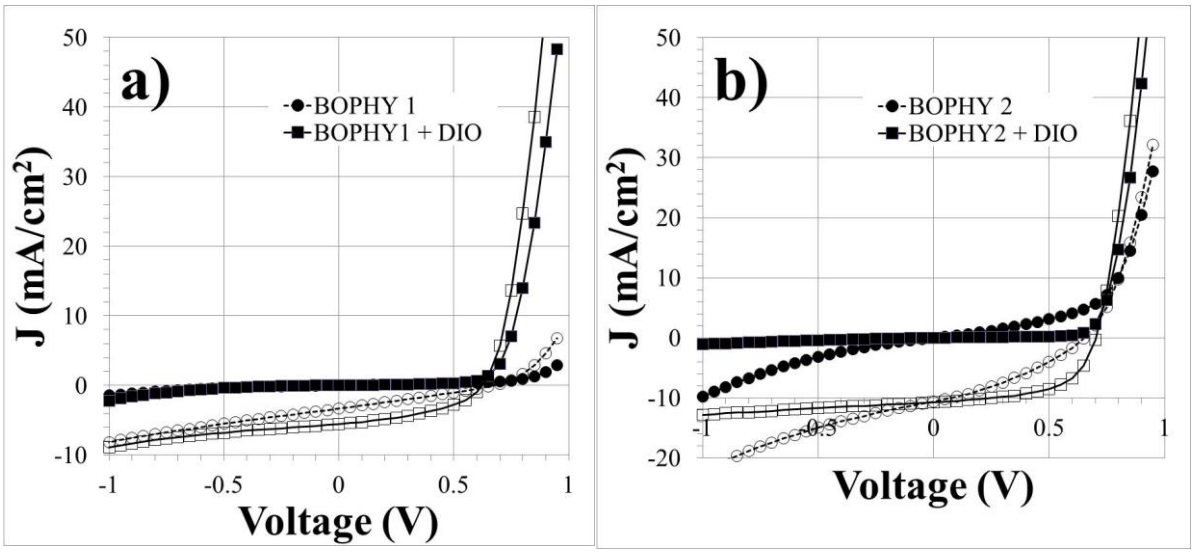

Table S5. Best photovoltaic performances measured for BOPHY-1 and BOPHY-2 using $PC_{71}BM$ as electron acceptor with a 1:1 ratio and Ca/Al as top cathode but with different experimental conditions.

Dye	*Solution Conc° (mg/mL)*	*Solvent*	*V_{oc} (V)*	*J_{sc} (mA/cm²)*	*FF (%)*	*PCE (%)*	*Annealing*
BOPHY-1	**10**	**$CHCl_3$+0.5% DIO**	**0.53**	**3.7**	**37**	**0.72**	**/**
BOPHY-1	15	$CHCl_3$+0.5 % DIO	0.63	5.5	43	1.51	/
BOPHY-1	10	$CHCl_3$	0.73	5.5	30	1.23	/
BOPHY-1	10	$CHCl_3$	0.73	5.2	29	1.08	1 min. 80°C
BOPHY-2	10	$CHCl_3$+0.4 % DIO	0.71	9.7	51	3.53	/
BOPHY-2	13	$CHCl_3$+0.4 % DIO	0.71	9.6	44	3.00	/
BOPHY-2	**10**	**$CHCl_3$+0.5% DIO**	**0.71**	**10.0**	**52**	**3.71**	**/**
BOPHY-2	10	$CHCl_3$+0.5 % DIO	0.71	9.5	53	3.58	5 min. 70°C

For **BOPHY-1**, increasing the solution concentration while keeping the spin-coating parameters unchanged, increases systematically the photovoltaic parameters (see for instance line 1 and 2 in Table S5). The active layer thickness is increased when increasing the solution concentration and consequently, the J_{sc} is also increased as the charge carrier mobility appears as sufficient for accurate charge extraction. This trend was observed up to a solution concentration of 15 mg/mL. The opposite was observed for **BOPHY-2** as increasing the solution concentration decreases the photovoltaic performances for every investigated experimental condition (see for instance line 5 and 6 in Table S5). Charge extraction for **BOPHY-2** seems to be problematic for thick devices, in line with the lower measured hole-mobility for this dye. The effect of a thermal annealing is less clear. In Table S5, the photovoltaic parameters decreases for both dyes after thermal treatment (line 3 and 4 for **BOPHY-1** and line 7 and 8 for **BOPHY-2**) while the best photovoltaic properties were observed after thermal annealing for **BOPHY-2** (Table 1). For similar experimental conditions (line 1 and 7 in Table S5), **BOPHY-2** always exhibit better photovoltaic performances with especially an almost three times higher J_{sc} value.

For the photovoltaic measurements under different light intensities, the short circuit current density (J_{sc}) is observed to deviate substantially from a linear dependence on the light intensity (Figure S17). This is a strong evidence of a device where charge carrier recombination is a strong charge carrier-loss process.[S10]

Figure S17. Normalized J_{sc} as a function of light power for one of the best performing cell using BOPHY-2 as electron-donnor in blend with $PC_{71}BM$ with a 1:1 ratio. Device structure: ITO/PEDOT:PSS/active layer/Ca/Al with a **BOPHY-2** concentration of 10 mg/mL in chloroform and with 0.3 vol% of DIO. The thick full-line represents a linear dependence of J_{sc} on the light intensity while the dotted line represents the sub-linear power fit with an exponent of 0.88.

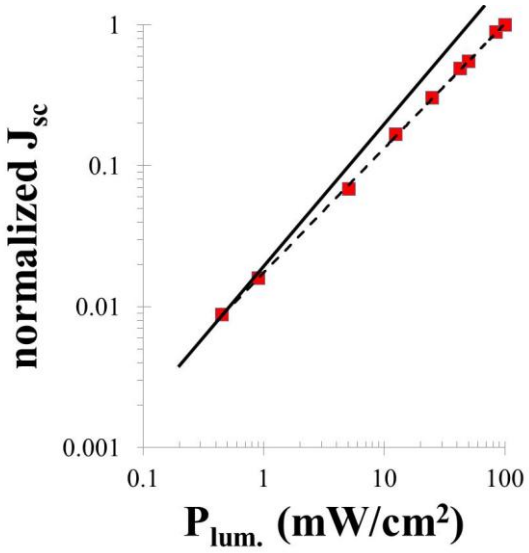

Figure S18. V_{oc} as a function of light power for one of the best performing cell using BOPHY-2 as electron-donnor in blend with $PC_{71}BM$ with a 1:1 ratio. Device structure: ITO/PEDOT:PSS/active layer/Ca/Al with a **BOPHY-2** concentration of 10 mg/mL in chloroform and with 0.3 vol% of DIO. The dotted line represents the expected variation of V_{oc} as a function of light power following equation 2.

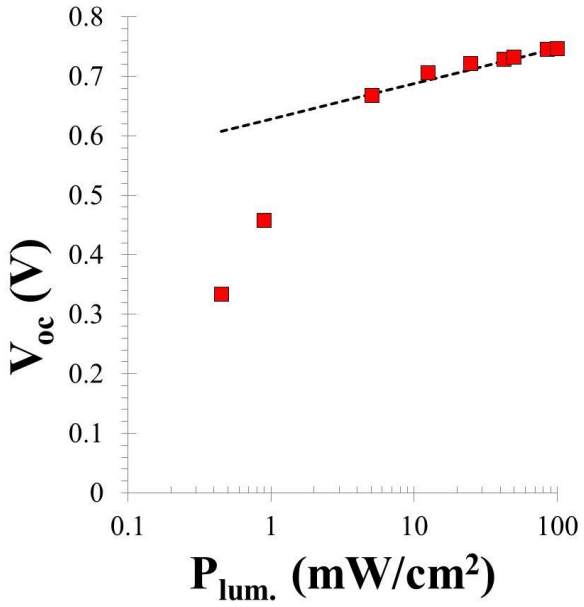

On the other hand, in a device with negligible leakage current and where only bimolecular recombination occurs, the open circuit voltage V_{oc} is expected to follow the equation:

$$V_{oc} = \frac{E_g}{q} - \frac{kT}{q} Ln\left(\frac{(1-P)\gamma N_c^2}{PG}\right) \ (equation\ 2)$$

where E_g is the band gap, q is the elementary charge, k is Boltzmann's constant, T is temperature, P is the dissociation probability of a bound electron-hole pair, γ is the bimolecular recombination rate coefficient, N_c is the effective density of states, and G is the photogeneration rate. G is the only term in Eq. (2) that depends on light intensity.[S10] Therefore, a system with only bimolecular recombination will exhibit a V_{oc} with a logarithmic dependence on light intensity with a slope of kT/q. as shown by the dotted line in Figure S18. At low light intensity, V_{oc} deviates from equation (2) as the assumption of a negligible leakage current is no more valid in our cells for a light intensity below 5 mW/cm^2. This last assertion is consolidated by the observation of the FF as a function of light power that drops sharply for light intensities below 5 mW/cm^2, as expected when the leakage-current could not be neglected anymore (Figure S19).[S11]

Figure S19. FF as a function of light power for one of the best performing cell using BOPHY-2 as electron-donnor in blend with $PC_{71}BM$ with a 1:1 ratio. Device structure: ITO/PEDOT:PSS/active layer/Ca/Al with a **BOPHY-2** concentration of 10 mg/mL in chloroform and with 0.3 vol% of DIO. The dotted line is an eye guide.

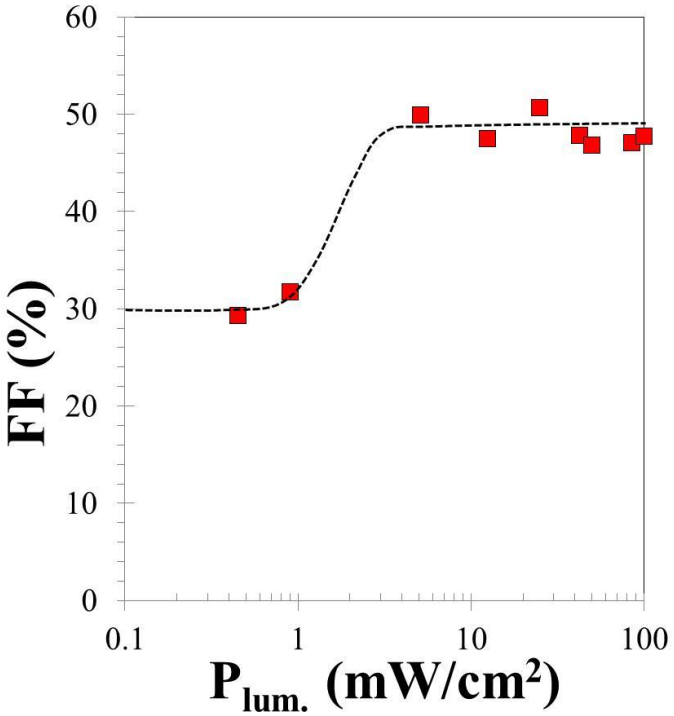

10) Atomic Force Microscopy (AFM) measurements.

Tapping-mode atomic force microscope (AFM) measurements were performed on a Nanoscope IIIa system commercialized by Veecor®. Measurements were performed directly on organic solar cell active layers.

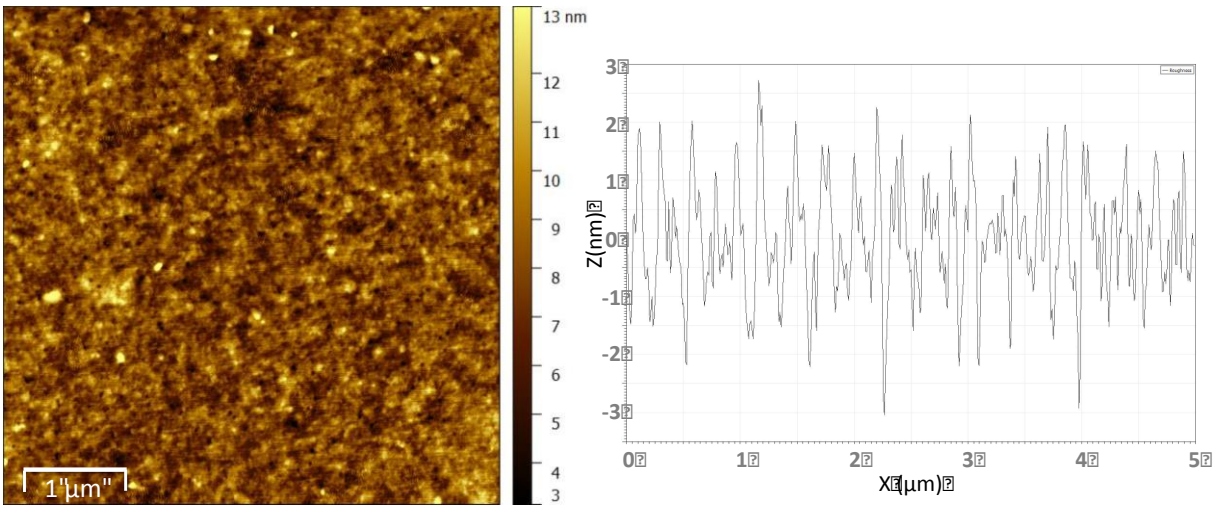

Figure S20. AFM topography image (left) with corresponding profile (right) of the best BOPHY 2:$PC_{71}BM$ device active layer.

11) Supplementary References

S1. Ziessel, R. *J. Am. Chem. Soc*. **2012**, *134*, 17404-17407.

S2. Rigaku/MSC *CrystalClear*. Rigaku/MSC Inc., 2009, The Woodlands, Texas, USA

S3. Sheldrick, G. M. Acta Cryst. **2008**, *A64*, 112–122.

S4. Sheldrick, G.M. Acta Cryst. **2015**, *C71***,** 3–8.

S5. Hübschle, C. B. Sheldrick, G. M. and Dittrich B. *J. Appl. Cryst.* **2011**, *44*, 1281-1284.

S6. Spek, A. L. (2009). Acta Cryst. **2009**, *D65*, 148-155.

S7. Burnett M N. and Johnson, C. K. ORTEP-III: Oak Ridge Thermal Ellipsoid Plot Program for Crystal Structure Illustrations, Oak Ridge National Laboratory Report ORNL-6895, 1996.

S8. Olmsted, J.; *J. Phys. Chem.* **1979**, *83*, 2581–2584.

S9. See *www.wavefun.com*

S10. Charge Carrier Recombination in Organic Solar Cells", C.M. Proctor, M. Kuik, T.-Q. Nguyen, *Prog. Polym. Sci.* **2013**, *38*, 1941-1960.

S11. Light intensity dependence of open-circuit voltage of polymer:fullerene solar cells", L.J.A. Koster, V.D. Mihailetchi, R. Ramaker, P.W.M. Blom, *Appl. Phys. Lett.* **2005**, *86*, 123509